CHAPTER 10

Two-bridge knots and links

In this chapter we will study in detail a class of knots and links that has particularly nice geometry, namely the class of 2-bridge knots and links. The key property of these links that we will explore is the fact that they admit a geometric triangulation that can be read off of a diagram, or an algebraic description of the link. In this chapter, we will define 2-bridge knots and links, describe their triangulations, and mention some of their geometric properties and consequences.

10.1. Rational tangles and 2-bridge links

In 1956, H. Schubert showed that the class of 2-bridge knots and links are classified by a rational number, and any continued fraction expansion of this number gives a diagram of the knot [**Schubert, 1956**]. In this section, we work through the description of 2-bridge knots and links via rational numbers. Additional references are [**Burde and Zieschang, 1985**] and [**Murasugi, 1996**].

First, we define tangles.

DEFINITION 10.1. A *tangle* is a 1-manifold properly embedded in a 3-ball B. That is, it is a collection of arcs with endpoints on ∂B and interiors disjointly embedded in the interior of B, possibly along with a collection of simple closed curves. For our purposes, we will consider only tangles consisting of two arcs, thus with four endpoints embedded on the boundary of a ball.

The simplest tangle is a rational tangle.

DEFINITION 10.2. A *rational tangle* is obtained by drawing two arcs of rational slope on the surface of a 4-punctured sphere (pillowcase), and then pushing the interiors into the 3-ball bounded by the 4-punctured sphere.

The tangles are called rational because they can be defined by a rational number, as follows. Recall that a rational number can be described by a

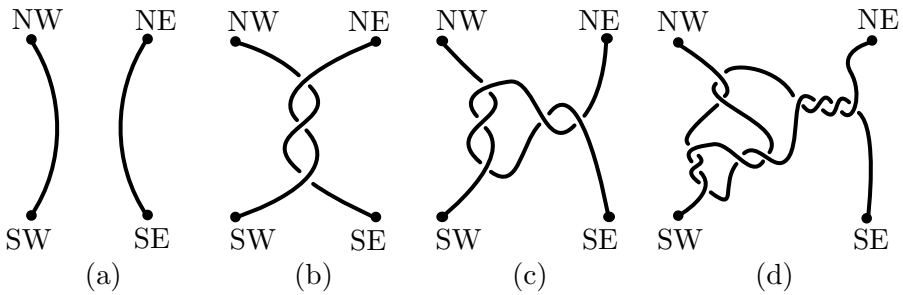

FIGURE 10.1. Building a rational tangle from the continued fraction $[4, -2, -2, 3]$. (Figure adapted from [**Finlinson and Purcell, 2016**])

continued fraction:

$$\frac{p}{q} = [a_n, a_{n-1}, \ldots, a_1] = a_n + \cfrac{1}{a_{n-1} + \cfrac{1}{\ddots + \cfrac{1}{a_1}}}.$$

Now, given a continued fraction $[a_n, \ldots, a_1]$, we will form a rational tangle. Start by labelling the four points on the pillowcase NW, NE, SW, and SE. If n is even, connect NE to SE and NW to SW by attaching two arcs as in figure 10.1(a). Perform a homeomorphism of B^3 that rotates the points NW and NE $|a_1|$ times, creating a vertical band of $|a_1|$ crossings in the two arcs. If $a_1 > 0$, rotate in a counterclockwise direction, so that the overcrossings of the result have positive slope. This is called a *positive crossing*. If $a_1 < 0$ rotate in a clockwise direction, so that overcrossings have negative slope, forming a *negative crossing*. In figure 10.1(b), three positive crossings have been added. After twisting, relabel the points NW, NE, SW, and SE to match their original orientation. Next, apply a homeomorphism of B^3 that rotates NE and SE $|a_2|$ times, adding crossings in a horizontal band. Again these crossings will be positive if $a_2 > 0$, and negative if $a_2 < 0$. Repeat this process for each a_i. When finished, we obtain a rational tangle. An example is shown in figure 10.1.

If n is odd, start with two arcs connecting NW to NE and SW to SE. In this case we add a horizontal band of crossings first, and then continue as before, alternating between horizontal and vertical bands for each a_i.

Any rational tangle may be built by this process. As a convention, we require that the left-most term a_n in the continued fraction expansion corresponds to a horizontal band of crossings. If we build a rational tangle ending with a vertical band, as in figure 10.1(b), then we insert a 0 into the corresponding continued fraction, representing a horizontal band of 0 crossings. For example, the continued fraction corresponding to the tangle in figure 10.1(b) is $[0, 3]$. This convention ensures that any continued fraction

completely specifies a single rational tangle. There are two trivial rational tangles, namely $0 = [0]$, with untwisted strands connecting NW to NE and SW to SE, and $\infty = [0, 0] = 0 + \frac{1}{0}$, with untwisted strands connecting NW to SW and NE to SE. The tangle ∞ is shown in figure 10.1(a).

PROPOSITION 10.3 ([**Conway, 1970**]). *Equivalence classes of rational tangles are in one-to-one correspondence with the set $\mathbb{Q} \cup \infty$. In particular, tangles $T(a_n, \ldots, a_1)$ and $T(b_m, \ldots, b_1)$ are equivalent if and only if the continued fractions $[a_n, \ldots, a_1]$ and $[b_m, \ldots, b_1]$ are equal.*

Proposition 10.3 allows us to put all our tangles into nice form.

COROLLARY 10.4. *Any rational tangle is equivalent to one of the form $T(a_n, \ldots, a_1)$ in which $a_i \neq 0$ for $1 \leq i < n$, and either all $a_i \geq 0$ or all $a_i \leq 0$.*

PROOF. This follows immediately from exercise 10.2. □

Thus we will assume that positive tangles have only positive crossings, and negative tangles have only negative crossings. In either case, this will make the tangle diagram alternating.

DEFINITION 10.5. The *numerator closure* $\text{num}(T)$ of a rational tangle T is formed by connecting NW to NE and SW to SE by simple arcs with no crossings. The *denominator closure* $\text{denom}(T)$ is formed by connecting NW to SW and NE to SE by simple arcs with no crossings.

DEFINITION 10.6. A *2-bridge knot or link* is the denominator closure of a rational tangle.

Notice that the denominator closure of the tangle $T(a_n, a_{n-1}, \ldots, a_1)$ is always equivalent to the denominator closure of the tangle $T(0, a_{n-1}, \ldots, a_1)$, since a_n corresponds to horizontal crossings that can simply be unwound after forming the denominator closure. Thus when we consider 2-bridge knots, we may assume that in our rational tangle, $a_n = 0$.

DEFINITION 10.7. The 2-bridge knot or link that is the denominator closure of the tangle $T(a_n, a_{n-1}, \ldots, a_1)$ (and $T(0, a_{n-1}, \ldots, a_1)$) is denoted by $K[a_{n-1}, \ldots, a_1]$.

The above discussion of twisting and taking denominator closure gives a nice correspondance between diagrams of 2-bridge knots and continued fraction expansions of rational numbers p/q with $|p/q| \leq 1$. This is summarised in the following lemma.

LEMMA 10.8. *Suppose $[0, a_{n-1}, \ldots, a_1]$ is a continued fraction with either $a_i > 0$ for all i or $a_i < 0$ for all i. Then the diagram of $K[a_{n-1}, \ldots, a_1]$ contains $n - 1$ twist regions, arranged left to right. The twist region on the far left contains $|a_1|$ crossings, with sign opposite that of a_1, the next twist region to the right containing $|a_2|$ crossings with sign the same as a_2, and so on, with the i-th twist region from the left containing $|a_i|$ crossings, with*

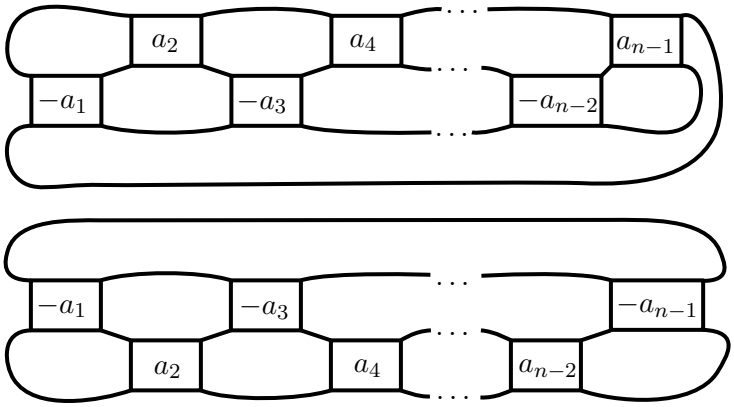

FIGURE 10.2. The diagram of $K[a_{n-1}, \ldots, a_1]$. Top: n odd; bottom: n even. Box labeled $\pm a_i$ denotes a (horizontal) twist region with $|a_i|$ crossings, with sign of the crossings equal to that of $\pm a_i$.

sign the same as a_i if i is even, and opposite a_i if i is odd. Twist regions connect as illustrated in figure 10.2.

PROOF. The tangle $T(0, a_{n-1}, \ldots, a_1)$ is obtained by forming horizontal or vertical bands of $|a_i|$ crossings, for $i = 1, \ldots, n-1$. Thus the diagram of the denominator closure has $n-1$ twist regions with the numbers of crossings as claimed. To put it into the form of figure 10.2, isotope the diagram by rotating vertical twist regions (with odd i) to be horizontal. This rotates odd twist regions to be horizontal, but with sign opposite that of a_i. □

LEMMA 10.9. *For a 2-bridge knot or link $K[a_{n-1}, \ldots, a_1]$, we may always assume $|a_1| \geq 2$ and $|a_{n-1}| \geq 2$.*

PROOF. Exercise. One way to see this is to consider the form of a 2-bridge knot or link with $|a_1| = 1$ or $|a_{n-1}| = 1$, and show that the corresponding twist region can be subsumed into another twist region. □

For the rest of this chapter, we will assume the conclusions of corollary 10.4 and lemma 10.9, namely that if $K[a_{n-1}, \ldots, a_1]$ is a 2-bridge knot or link, then either $a_i > 0$ for all i or $a_i < 0$ for all i, and $|a_{n-1}| \geq 2$ and $|a_1| \geq 2$.

10.2. Triangulations of 2-bridge links

We now describe a way to triangulate 2-bridge link complements that was first observed by Sakuma and Weeks [**Sakuma and Weeks, 1995**]. A description was also given by Futer in the appendix of [**Guéritaud, 2006**]; we base our exposition here off of the latter paper.

Consider again our construction of a rational tangle. We started with two strands in a 4-punctured sphere, or pillowcase. To form each crossing, we

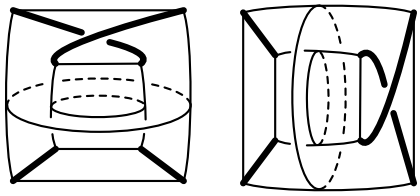

FIGURE 10.3. Vertical (left) and horizontal (right) blocks of the form $S \times I$. The 4-punctured spheres on the outside and inside correspond to $S \times \{1\}$ and $S \times \{0\}$, respectively

either rotate the points NE and NW or the points NE and SE. In the former case, we call the crossing a *vertical* crossing, and in the latter a *horizontal* crossing. For all but the first crossing in a tangle, adding a crossing can be seen as stacking a region $S^2 \times I$ to the outside of a pre-existing tangle, where $S^2 \times I$ contains four strands, two of them forming a crossing. Positive vertical and horizontal crossings in $S^2 \times I$ are shown in figure 10.3, negative ones will be in the opposite direction. If we drill the four strands from $S^2 \times I$, the region becomes $S \times I$, where S is a 4-punctured sphere.

LEMMA 10.10. *Let $K := K[a_{n-1}, \ldots, a_1]$ be a 2-bridge link and let C denote the number of crossings of K; so $C = |a_1| + \cdots + |a_{n-1}|$. Assume either $a_i < 0$ for all i or $a_i > 0$ for all i, and $|a_1| \geq 2$ and $|a_{n-1}| \geq 2$. Let N be the manifold obtained from the complement $S^3 - K$ by removing a ball neighborhood of the first and last crossings, and let S denote the 4-punctured sphere. Then N is homeomorphic to $S \times [a, b]$, obtained from stacking $C - 2$ copies of $S \times I$ end to end, with each copy of $S \times I$ corresponding to either a horizontal or vertical crossing.*

- *If n is even, the first $a_1 - 1$ copies of $S \times I$ are vertical, followed by a_2 horizontal copies, a_3 vertical, etc, finishing with $a_{n-1} - 1$ vertical copies of $S \times I$.*
- *If n is odd, the first $a_1 - 1$ copies of $S \times I$ are horizontal, followed by a_2 vertical copies, a_3 horizontal, etc, finishing with $a_{n-1} - 1$ vertical copies.*

The i-th copy of $S \times I$ is glued along $S \times \{1\}$ to $S \times \{0\}$ on the $(i+1)$-st copy, $i = 2, 3, \ldots, C - 1$. □

An example of lemma 10.10 is shown in figure 10.4.

We will obtain a triangulation of a 2-bridge link complement by first finding a triangulation of the manifold N in lemma 10.10. To do so, we will consider each of the blocks $S \times I$ separately, and then consider how they fit together.

Denote the blocks of lemma 10.10 by $S_2 \times I, S_3 \times I, \ldots, S_{C-1} \times I$, where $S_i \times I$ corresponds to the i-th crossing of the tangle. In the description below, we will consider the case that all crossings are positive, i.e. $a_j > 0$ for all j, so that if the i-th crossing is vertical, then $S_i \times I$ has the form of

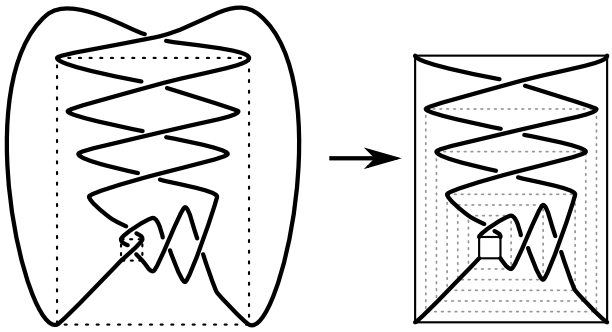

FIGURE 10.4. On the left is $K[4,2,2]$. On the right, remove neighborhoods of inside and outside crossings to obtain a manifold homeomorphic to $S \times [a,b]$. Each crossing is contained in a block $S \times I$ of the form of figure 10.3

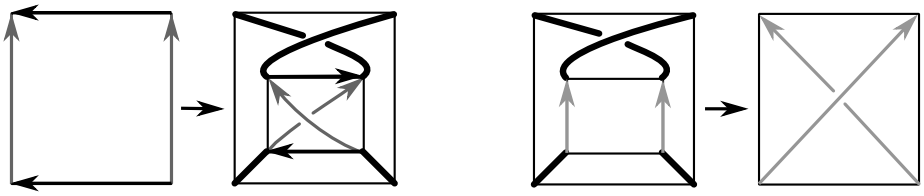

FIGURE 10.5. Effect on ideal edges of isotopies between $S_i \times \{1\}$ and $S_i \times \{0\}$

the left of figure 10.3, and if it is horizontal, then $S_i \times I$ has the form of the right. The case of all negative crossings will be similar.

In $S_i \times I$, the 4-punctured sphere S_i is embedded at any level $S_i \times \{t\}$. We will focus in particular on $S_i \times \{0\}$ and $S_i \times \{1\}$.

LEMMA 10.11. *There is an ideal triangulation of S_i such that when we isotope the triangulation to $S_i \times \{1\}$, edges are horizontal (from NE to NW and from SE to SW), vertical (from SW to NW and from SE to NE), and diagonal, and when we isotope the triangulation to $S_i \times \{0\}$, edges are still horizontal, vertical, and diagonal, but the diagonals are opposite those of $S_i \times \{1\}$.*

PROOF. First consider the outside, $S_i \times \{1\}$. Draw vertical and horizontal ideal edges on $S_i \times \{1\}$; that is, draw horizontal edges from NE to NW and from SE to SW, and draw vertical edges from SE to NE and from SW to NW. Now isotope from $S_i \times \{1\}$ through $S_i \times \{t\}$ inside to $S_i \times \{0\}$, and track these ideal edges through the isotopy.

In the case that $S_i \times I$ has a vertical crossing, as on the left of figure 10.3, notice that the isotopy takes the horizontal edges in $S_i \times \{1\}$ to horizontal edges in $S_i \times \{0\}$, but it takes vertical edges in $S_i \times \{1\}$ to diagonal edges in $S_i \times \{0\}$, as shown on the left of figure 10.5. Now consider the vertical edges in $S_i \times \{0\}$, i.e. the ideal edges running from SE to NE and SW to NW on

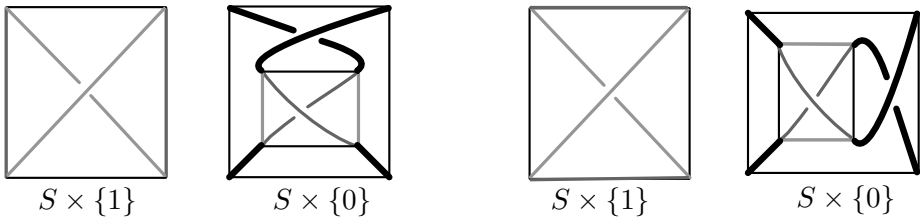

FIGURE 10.6. Triangulation of $S_i \times \{1\}$ and $S_i \times \{0\}$, shown for both horizontal and vertical (positive) crossings.

the inside of the block. When we isotope $S_i \times \{0\}$ to $S_i \times \{1\}$, notice that these edges become diagonal edges on $S_i \times \{1\}$, as shown on the right of figure 10.5. Notice that these diagonals are exactly opposite the diagonals on the inside on the left of the figure.

When $S_i \times I$ has a horizontal crossing, as on the right of figure 10.3, the vertical ideal edges in $S_i \times \{1\}$ are isotopic to vertical edges in $S_i \times \{0\}$. Horizontal edges on $S_i \times \{1\}$ isotope to diagonal edges on $S_i \times \{0\}$, and horizontal edges on $S_i \times \{0\}$ isotope to diagonal edges on $S_i \times \{1\}$. Again the diagonal edges have opposite slopes on the inside and outside.

In either case, add all horizontal and vertical edges to S_i on $S_i \times \{1\}$ and add all horizontal and vertical edges to S_i on $S_i \times \{0\}$. Since either horizontal or vertical edges are duplicated, we add six ideal edges total. This is the triangulation claimed in the lemma. □

The triangulation of $S_i \times \{1\}$ and $S_i \times \{0\}$ for both vertical and horizontal crossings is shown in figure 10.6. (We have removed the arrows from the edges as we will not need to work with directed edges, and keeping track of direction will unnecessarily complicate the discussion.) Note the ideal edges cut $S_i \times \{1\}$ into four ideal triangles: two on the front and two on the back. Similarly, these ideal triangles can be isotoped to the inside $S_i \times \{0\}$, giving two triangles on the front and two on the back, although notice that the isotopy does not take both triangles in the front of $S_i \times \{1\}$ to triangles in the front of $S_i \times \{0\}$.

So far we only have ideal triangles on surfaces S_i, and no ideal tetrahedra. The ideal tetrahedra are obtained when we put blocks $S_{i-1} \times I$ and $S_i \times I$ together, and we now describe how this works.

LEMMA 10.12. *With S_{i-1} and S_i triangulated as in lemma 10.11, gluing $S_{i-1} \times I$ to $S_i \times I$ by identifying $S_{i-1} \times \{1\}$ and $S_i \times \{0\}$ gives rise to two ideal tetrahedra, each with two faces on S_{i-1} and two on S_i.*

PROOF. Consider the triangulations of $S_{i-1} \times \{1\}$ and $S_i \times \{0\}$ from lemma 10.11, shown in figure 10.6. Notice that the diagonal edges of $S_{i-1} \times \{1\}$ are exactly opposite the diagonal edges of $S_i \times \{0\}$, and so these edges do not match up. The horizontal and vertical edges on $S_{i-1} \times \{1\}$ and $S_i \times \{0\}$ can be identified, but the diagonal edges cannot. To keep these edges

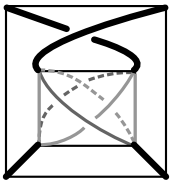

FIGURE 10.7. When blocks are glued, diagonals of the triangulated surfaces S_i and S_{i-1} are as shown.

embedded, we view the diagonals of $S_{i-1} \times \{1\}$ as inside of the diagonals of $S_i \times \{0\}$, as shown in figure 10.7.

With horizontal and vertical edges identified, notice that the interior of the region between $S_{i-1} \times \{1\}$ and $S_i \times \{0\}$ lies in two components: one on the front of the figure, and one on the back. Each of these components is bounded by four triangular faces, six ideal edges, and four ideal vertices; each is an ideal tetrahedron as desired. □

By lemma 10.12, when we glue $S_i \times I$ to $S_{i+1} \times I$, we obtain two additional tetrahedra, and these will be attached along S_i to the two tetrahedra from $S_i \times I$ and $S_{i-1} \times I$. Thus as we run from $S_2 \times I$ out to $S_{C-1} \times I$, we obtain pairs of tetrahedra for each gluing of blocks, and these are glued inside to outside to form a triangulation of $N \cong S \times [a, b]$.

Now, at this stage, we have a triangulation of N, but there will be four triangular faces on the very inside corresponding to S_2 that are unglued, and four triangular faces on the very outside corresponding to S_{C-1} that are unglued. To complete the description of the triangulation of the 2-bridge link complement, we need to describe what happens at the outermost and innermost crossings, e.g. on the left of figure 10.4.

PROPOSITION 10.13. *Let $K := K[a_{n-1}, \ldots, a_1]$ be a 2-bridge link with at least two twist regions, with either $a_i > 0$ for all $1 \leq i \leq n-1$, or $a_i < 0$ for all i. Assume $|a_1| \geq 2$ and $|a_{n-1}| \geq 2$. Let $C = |a_1| + \cdots + |a_{n-1}|$ denote the number of crossings of K. Then $S^3 - K$ has a decomposition into $2(C-3)$ ideal tetrahedra denoted by T_i^1, T_i^2, for $i = 2, \ldots, C-2$.*

- *For $2 \leq i \leq C-2$, the tetrahedra T_i^1 and T_i^2 each have two faces on S_i and two on S_{i+1}.*
- *The two faces of T_2^1 on S_2 glue to the two faces of T_2^2 on S_2.*
- *Similarly, the two faces of T_{C-2}^1 on S_{C-1} glue to the two faces of T_{C-2}^2 on S_{C-1}.*

PROOF. The tetrahedra come from the triangulation of N. By the previous lemmas, there are two tetrahedra for each pair of adjacent crossings, omitting the first and last, thus $2(C-3)$ tetrahedra. By lemma 10.12, each tetrahedron in each pair has two faces on S_i and two on S_{i+1}, where $S_i \times I$ and $S_{i+1} \times I$ are blocks corresponding to the two adjacent crossings. We

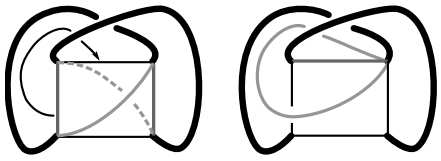

FIGURE 10.8. Identifying triangles of the outermost 4-punctured sphere

label the tetrahedra T_2^1, T_2^2, T_3^1, T_3^2, ..., T_{C-2}^1, T_{C-2}^2, so that the first item is satisfied.

It remains to show that the innermost and outermost tetrahedra, T_2^1, T_2^2 and T_{C-2}^1, T_{C-2}^2, glue as claimed. We will focus on the outermost tetrahedra here. The innermost case is similar, but we leave its description to the reader.

For the outermost crossing, recall that we may assume our 2-bridge knot is the denominator closure of a tangle $T(a_n, a_{n-1}, \ldots, a_1)$ with $a_n = 0$. Thus the outermost crossing will be vertical, not horizontal. Hence we restrict to pictures with a single vertical crossing on the outside.

The outermost 4-punctured sphere S_{C-1} will be triangulated as shown on the left of figure 10.8. Notice that when we add the outside crossing as shown, vertical edges and horizontal edges all become isotopic and hence are identified, by isotopies swinging the endpoints around the strand of the crossing. One such isotopy is indicated by the small arrow on the left of figure 10.8.

The diagonal edges are not identified to horizontal or vertical edges. When we follow the isotopy of figure 10.8, the diagonal edge in the front wraps once around a strand of the knot, as shown on the right of figure 10.8. Thus the triangle in the upper left corner of S_{C-1} maps under the isotopy to a triangle with two of its edges identified, looping around a strand of the 2-bridge knot.

Now consider the triangle in front in the lower right corner. We will isotope the triangle by dragging its vertex on the SE corner around the strand of the knot to the NW corner. If we perform this isotopy while holding the diagonal fixed, note that the lower left triangle flips around backwards to be identified to the upper right triangle in the front. Thus the two triangles on the front of $S_{C-1} \times \{1\}$ will be identified under isotopy. Similarly for the two back triangles.

Thus inserting the outermost crossing identifies the four outside triangular faces of the outermost tetrahedra in pairs.

The tetrahedra T_{C-2}^1 and T_{C-2}^2 have triangular faces on S_{C-1}, shown in figure 10.7. One of these, say T_{C-2}^1, will lie in front in that figure and one will lie in back.

However, note that in figure 10.7, we have isotoped the surface S_{C-1} to be in the position of $S_{C-1} \times \{0\}$, while in figure 10.8, when we glue faces of S_{C-1}, we have isotoped S_{C-1} to be in the position of $S_{C-1} \times \{1\}$. Isotoping

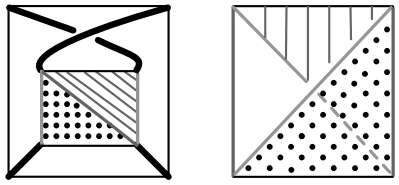

FIGURE 10.9. Locations of faces of T^1_{C-2} under isotopy from $S \times \{0\}$ to $S \times \{1\}$

from $S_{C-1} \times \{0\}$ to $S_{C-1} \times \{1\}$ will move the faces of T^1_{C-2} and T^2_{C-2}. In particular, the face of T^1_{C-2} lying on the upper right of figure 10.7 will be moved by isotopy to lie in the back on the upper right, and the face of T^1_{C-2} lying in the lower left will be moved by isotopy to lie in front, in the lower right. See figure 10.9.

Thus the identification of triangles on the outside identifies faces of T^1_{C-2} to faces of T^2_{C-2}. □

10.2.1. The cusp triangulation. Now we consider the view of the tetrahedra from a cusp. Consider first the manifold N with ball neighborhoods of the first and last crossings removed. The manifold N is homeomorphic to the product of a 4-punctured sphere and a closed interval. Note that in N, there are four distinct cusps, corresponding to the product of I and the four distinct punctures of the 4-punctured sphere. Note that each cusp meets each 4-punctured sphere S_i, and that a curve on S_i running around the puncture forms a meridian. Finally, note that between each S_i and S_{i+1} lie two tetrahedra, as in figure 10.7. Each tetrahedron has exactly one ideal vertex on each of the four cusps. Thus the cusp triangulation of N consists of four disjoint cusp neighborhoods. Each cusp neighborhood meets each S_i, in the same order, and each cusp neighborhood meets each tetrahedron in the decomposition in the same order. Thus the four cusp triangulations look identical at this stage, at least combinatorially. We will create one of these four cusps.

In order to see the pattern of tetrahedra in one of these cusps, note that there will be a stack of triangles in each cusp, each triangle corresponding to the tip of a tetrahedron. By proposition 10.13, the triangles will be sandwiched between 4-punctured spheres S_i and S_{i+1}, with the bottom of the stack of triangles bounded by S_2 and the top by S_{C-1}. (Recall that the 4-punctured sphere S_i actually lies in a block $S_i \times I$, so when we refer to S_i in the following it may be helpful to recall that we are referring to a surface isotopic to $S_i \times \{t\}$ for appropriate t.)

When we run along a meridian of the cusp on S_i, we stay on edges of the cusp triangulation. Moreover, note that we pass over exactly three ideal edges; see the left of figure 10.10. Thus in the cusp triangulation, running along such a meridian on the surface S_i will correspond to running over three

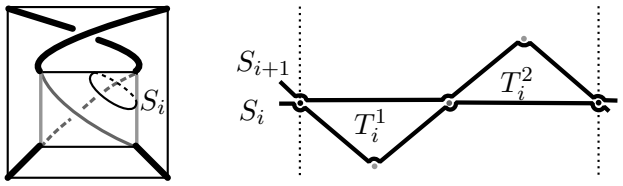

FIGURE 10.10. Form of two meridians running over S_i and S_{i+1}

edges of triangles. This is shown in figure 10.10 for S_i. The vertical dotted lines indicate boundaries of a fundamental region for the cusp torus; in this case running from one dotted line to the other corresponds to a meridian.

When the i-th, $(i+1)$-st, and $(i+2)$-nd blocks are all vertical crossings, note that the surfaces S_i, S_{i+1}, and S_{i+2} will all share an edge; a horizontal edge in figure 10.6. Similarly adjacent horizontal crossings also lead to surfaces sharing an edge.

NOTATION 10.14. In the cusp triangulation we see 4-punctured spheres $S_2, \ldots, S_{C-1}$. Give the label R to each 4-punctured sphere S_i corresponding to a block $S_i \times I$ containing a horizontal crossing. Give the label L to each corresponding to a block containing a vertical crossing. A tetrahedron that lies between layers labeled R and L is called a *hinge tetrahedron*.

The labels R and L are given for historical reasons; they refer to moves to the right and left for a path in the Farey graph given by the rational number of our tangle. We won't delve into the history of this notation here, but we will use this notation for ease of reference with other literature. For more information see [**Guéritaud, 2006**].

EXAMPLE 10.15. A cusp triangulation for an example N is shown in figure 10.11. That figure follows some standard conventions. Because we have many surfaces S_i, we connect edges of S_i to form a single connected jagged line, identifiable as one surface in the cusp, and put a little space between multiple such surfaces at a vertex they share. We also put vertices of the triangles in two columns (in a fundamental domain). Finally, we shade the hinge layers.

Note in the figure as we move inside to out, we move from the bottom of the cusp triangulation to the top. Tetrahedron T_2^1 lies between surfaces S_2 associated with the second innermost crossing (vertical, L) and S_3 associated with the third innermost crossing (horizontal, R). It is a hinge tetrahedron. Tetrahedron T_3^1 lies between S_3 and S_4, both of which are associated with horizontal crossings, R. Note there is an ideal edge shared by all three surfaces S_2, S_3, and S_4, and this corresponds to a shared vertex of T_2^1 and T_3^1 in the cusp triangulation (in the center).

Now we determine what happens to cusps when we put in the innermost and outermost crossings. At the outermost crossing, note that the cusp corresponding to the vertex SE becomes identified with the cusp corresponding

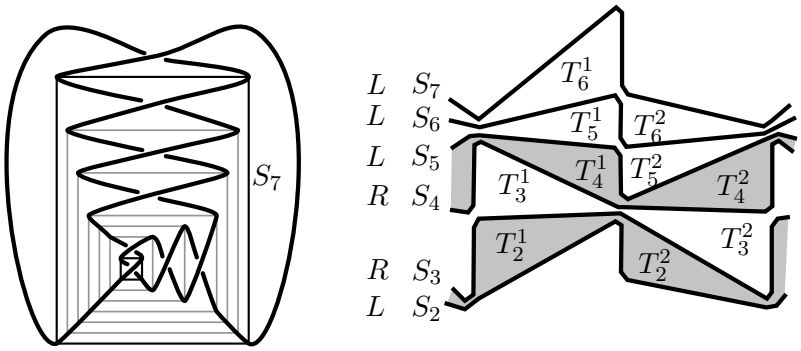

FIGURE 10.11. On the right is shown the cusp triangulation of one of the four cusps of N on the left

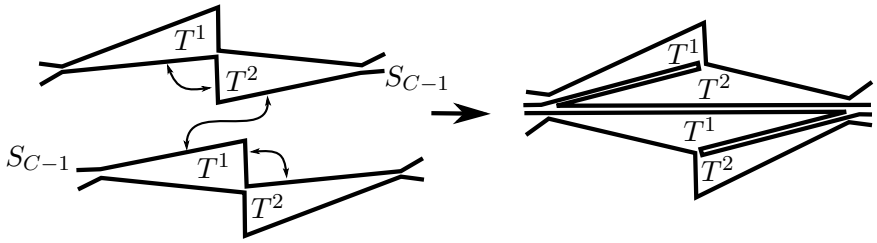

FIGURE 10.12. Gluing tetrahedra across S_{C-1} yields a hairpin turn

to the vertex NW, and similarly for SW and NE. Thus the four identical cusp triangulations we have obtained so far will be glued. Recall that the gluing is along triangle faces of S_{C-1} in the case of the outermost crossing. The faces of T^1_{C-2} are glued to faces of T^2_{C-2}. The result is a "folding" of triangles. See figure 10.12. We call this a *hairpin turn*.

If K is a knot, if we follow a longitude of the cusp, starting at one of the corners of S_2, we will see 4-punctured spheres $S_2, S_3, \ldots, S_{C-2}$, then a hairpin turn on S_{C-1} corresponding to the outside crossing as in figure 10.12. Continuing, we will pass $S_{C-2}, S_{C-3}, \ldots, S_3$, then another hairpin turn on S_2 corresponding to the inside crossing, then $S_3, \ldots, S_{C-1}$ and a hairpin turn, and finally $S_{C-2}, \ldots, S_3$ and the original S_2 with a hairpin turn. A hairpin turn appears in the cusp triangulation as a single edge stretching across a meridian, adjacent to two triangles whose third vertex is 3-valent.

We summarize:

PROPOSITION 10.16. *Let $K := K[a_{n-1}, \ldots, a_1]$ be a 2-bridge knot with at least two twist regions, such that either $a_i > 0$ for all i, or $a_i < 0$ for all i, and $|a_1| \geq 2$ and $|a_{n-1}| \geq 2$. Let $C = |a_1| + \cdots + |a_{n-1}|$ denote the number of crossings of K. The cusp triangulation of K has the following properties.*

- *It is made of four pieces, each piece bookended by hairpin turns corresponding to 4-punctured spheres S_2 and S_{C-1}. Between lies*

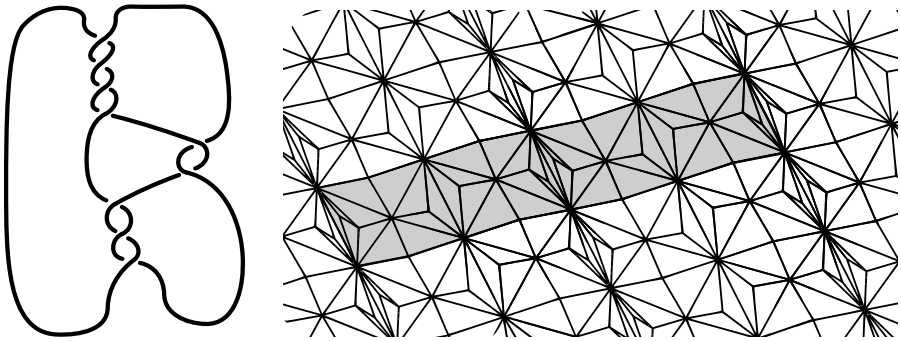

FIGURE 10.13. An example of a 2-bridge knot and its cusp triangulation from SnapPy. The shaded region shows a fundamental domain for the cusp torus, stretching from one hairpin turn through three others back to the same hairpin turn.

a sequence of 4-punctured spheres $S_3, \dots, S_{C-2}$. We call the 4-punctured spheres zig-zags.

- *The first and third pieces are identical; the second and fourth are also identical and given by rotating the first piece* 180° *about a point in the center of the edge of the final hairpin turn (and swapping some labels T_i^1 as T_i^2). Thus the second and fourth pieces follow the first in reverse.*
- *When running in a longitudinal direction, the first piece begins with $|a_{n-1}| - 1$ zig-zags labeled L; the first of these is S_{C-1}, the hairpin turn corresponding to the outside crossing of the knot. These zig-zags are followed by $|a_{n-2}|$ zig-zags labeled R, then $|a_{n-3}|$ labeled L, and so on. If n is even, finish with $|a_1| - 1$ zig-zags labeled L, the last of which is the final hairpin turn, corresponding to S_2 at the inside crossing. If n is odd, the final $|a_1| - 1$ zig-zags will be labeled R.*
- *A meridian follows a single segment of the zig-zag in a hairpin turn, or three segments of any other zig-zag.*

Note we see each S_i exactly four times, including seeing S_2 twice for each of the two hairpin turns in the cusp triangulation corresponding to the inside crossing, and seeing S_{C-1} twice for each hairpin turn corresponding to the outside crossing.

An example sketched by SnapPy ([**Culler et al., 2016**]) is shown in figure 10.13.

10.3. Positively oriented tetrahedra

The triangulation described in the last section has nice geometry. In particular, when the 2-bridge link has at least two twist regions, we can find angle structures on the triangulation. These can be used to prove that

the 2-bridge link is hyperbolic (corollary 10.20), and to show that in the complete hyperbolic structure on the link complement, the tetrahedra are all geometric. Thus we will obtain our first infinite class of knots and links with known geometric triangulations.

The main theorem of the next two sections is theorem 10.17, below. It was originally proved by Futer in the appendix to [**Guéritaud, 2006**].

THEOREM 10.17. *Let K be a 2-bridge knot or link complement with a reduced alternating diagram with at least two twist regions. Let $\mathcal{T}$ be the triangulation of $S^3 - K$ as described above. Then $S^3 - K$ is hyperbolic, and in the complete hyperbolic structure on $S^3 - K$, all tetrahedra of $\mathcal{T}$ are positively oriented.*

The proof of theorem 10.17 uses angle structures on $\mathcal{T}$, as in definition 8.21, and is done in two steps. First, the space of angle structures $\mathcal{A}(\mathcal{T})$ is shown to be non-empty. In theorem 8.28, we showed that the existence of an angle structure is enough to conclude that the manifold admits a hyperbolic structure. We conclude that these 2-bridge link complements are hyperbolic.

Second, in the next section, we show that the volume functional cannot achieve its maximum on the boundary of $\mathcal{A}(\mathcal{T})$. This is all that is needed: because the volume functional is strictly concave down on $\mathcal{A}(\mathcal{T})$ (lemma 9.15), it achieves a maximum in the interior of $\mathcal{A}(\mathcal{T})$. By theorem 9.13, the maximum corresponds to the complete hyperbolic structure, and at that structure, all angles are strictly positive, meaning all tetrahedra are geometric — positively oriented.

PROPOSITION 10.18. *Let $\mathcal{T}$ be the triangulation of a 2-bridge knot or link complement with at least two twist regions, as described above. Then the space of angle structures $\mathcal{A}(\mathcal{T})$ is nonempty.*

The proof of the proposition is not hard, but requires additional notation. First, we need to label the angles of each of the tetrahedra constructed in the previous section. Remember that the tetrahedra were constructed in pairs, and the pairs of tetrahedra lie between two 4-punctured spheres of the manifold $N = S \times [a, b]$, as in figure 10.7. In order to show some angle structure exists, we will first assume that the angles on each of these pairs of tetrahedra agree. Let z_i denote the angle on the outside diagonal edges of tetrahedra T_i^1 and T_i^2. Because opposite edges have the same angle, z_i is also the angle on the inside diagonal edge. Denote the angle at the horizontal edges by x_i and the angle at vertical edges by y_i. We may add these angles to the cusp triangulation. The cusp triangulation was obtained by adding layers of zig-zagging 4-punctured spheres. Each 4-punctured sphere shares two edges with the previous 4-punctured sphere, and has one new edge. In the cusp triangulation, this forms a sequence of triangles in which two vertices are shared, but one new vertex is added. The new vertex corresponds to the diagonal edge, so is labeled z_i. Note that angles labeled x_i are glued

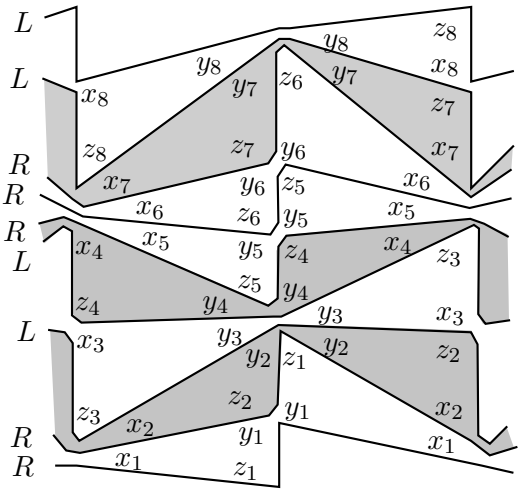

FIGURE 10.14. Labels on the cusp triangulation of $N = S \times [a, b]$ for an example

together, as are angles labeled y_i. Finally, we have oriented tetrahedra so that angles read x_i, y_i, z_i in clockwise order around a cusp triangle. This completely determines the labeling on all the cusp triangles of $N = S \times [a, b]$. An example is shown in figure 10.14.

In the example, a 4-punctured sphere corresponding to a horizontal crossing is labeled R, and one corresponding to a vertical crossing is labeled L, as in notation 10.14.

Now (x_i, y_i, z_i) give us labels for angles of all the tetrahedra on the 2-bridge link complement. We will need $x_i + y_i + z_i = \pi$ for each i to satisfy condition (8.21) of the definition of an angle structure, definition 8.21. We also need sums of angles around edge classes to be 2π.

Away from hairpin turns, the edge gluings of $S^3 - K$ agree with those of $N = S \times [a, b]$, so we will first consider angle sums around edges of N, simplifying these conditions to a system of equations in terms of the z_i alone, then deal with hairpin turns later. There will be four cases depending on whether the i-th tetrahedron lies between two horizontal crossings, two vertical crossings, a horizontal followed by a vertical crossing, or a vertical followed by a horizontal crossing. These cases are denoted by RR, LL, RL, and LR, respectively.

The labels for two consecutive LL 4-punctured spheres are shown in figure 10.15. Note in this case, there is a 4-valent vertex in the cusp triangulation (or 4-valent ideal edge in the decomposition into tetrahedra). In order for the angle sum around this edge to be 2π, we need $2x_i + z_{i+1} + z_{i-1} = 2\pi$, or $x_i = \frac{1}{2}(2\pi - z_{i-1} - z_{i+1})$. Then in order for $x_i + y_i + z_i = \pi$, we need $y_i = \frac{1}{2}(z_{i-1} - 2z_i + z_{i+1})$.

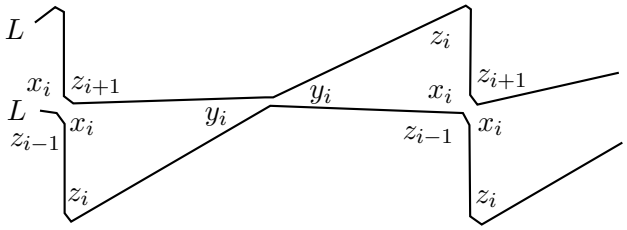

FIGURE 10.15. Labels in the LL case

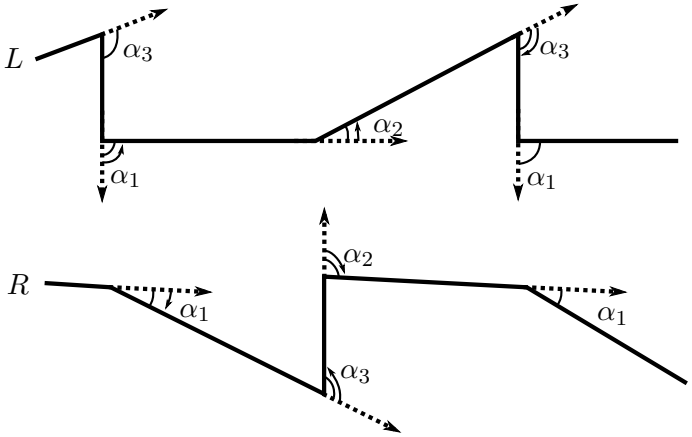

FIGURE 10.16. Pleating angles for 4-punctured spheres

A similar picture occurs in the RR case. Again there is a 4-valent vertex, and reading the labels around that vertex we find that we need the formulas $y_i = \frac{1}{2}(2\pi - z_{i-1} - z_{i+1})$, and $x_i = \frac{1}{2}(z_{i-1} - 2z_i + z_{i+1})$.

In the LR and RL cases, there is not a single edge all of whose labels we can read off the diagram. In these cases, we find restrictions by considering *pleating angles*. Pleating angles α_1, α_2, and α_3 are the angles determining the bending of the pleated 4-punctured sphere. They are shown for 4-punctured spheres labeled L and R in figure 10.16.

LEMMA 10.19. *If the angle structure gives a Euclidean structure on the cusp, then it will be the case that pleating angles as in figure 10.16 satisfy* $\alpha_1 + \alpha_2 - \alpha_3 = 0$.

PROOF. Exercise. □

To find an angle structure, we will assume this pleating condition holds in the LR and RL case.

The LR labels are shown in figure 10.17. Note that the pleating angles for the 4-punctured sphere at the bottom of the diagram are $\alpha_1 = \pi - z_i$, $\alpha_2 = \pi - (2y_i + z_{i+1})$, and $\alpha_3 = \pi - z_{i-1}$. Thus the condition $\alpha_1 + \alpha_2 - \alpha_3 = 0$ implies $y_i = \frac{1}{2}(\pi + z_{i-1} - z_i - z_{i+1})$. The pleating angles on the 4-punctured sphere on the top of the diagram in figure 10.17 are $\alpha_1 = \pi - (2x_i + z_{i-1})$,

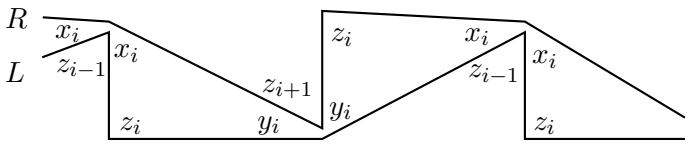

FIGURE 10.17. Labels in the LR case

	LL	RR
x_i	$\frac{1}{2}(2\pi - z_{i-1} - z_{i+1})$	$\frac{1}{2}(z_{i-1} - 2z_i + z_{i+1})$
y_i	$\frac{1}{2}(z_{i-1} - 2z_i + z_{i+1})$	$\frac{1}{2}(2\pi - z_{i-1} - z_{i+1})$
z_i	z_i	z_i

	LR	RL
x_i	$\frac{1}{2}(\pi - z_{i-1} - z_i + z_{i+1})$	$\frac{1}{2}(\pi + z_{i-1} - z_i - z_{i+1})$
y_i	$\frac{1}{2}(\pi + z_{i-1} - z_i - z_{i+1})$	$\frac{1}{2}(\pi - z_{i-1} - z_i + z_{i+1})$
z_i	z_i	z_i

TABLE 10.1. Label conditions in terms of the z_i

$\alpha_2 = \pi - z_i$, and $\alpha_3 = \pi - z_{i+1}$. Thus the pleating condition for this 4-punctured sphere gives $x_i = \frac{1}{2}(\pi - z_{i-1} - z_i + z_{i+1})$. Conditions can be obtained in a similar manner in the RL case.

In summary, away from hairpin turns, labels must satisfy the conditions given in table 10.1.

Notice this allows us to express x_i and y_i in terms of z_{i-1}, z_i, and z_{i+1} alone. Note also that the sum of the angles $x_i + y_i + z_i = \pi$ in each case.

Finally, we claim that with the conditions in table 10.1, the angle sum around each edge in N is 2π. To see this, note first that we have constructed the angles so that the sum is 2π around 4-valent edges. We now check the remaining edges. The angle sum around one such edge will be

$$z_{j-1} + 2x_j + \sum_{i=j+1}^{k-1} 2x_i + 2x_k + z_{k+1},$$

where j and k are indices of hinge tetrahedra, with j between LR and k between RL, and $j < k$, and all 4-punctured spheres labeled R between them; refer to figure 10.14. By the formulas in the tables, this is

$$z_{j-1}+\pi-z_{j-1}-z_j+z_{j+1}+\sum_{i=j+1}^{k-1}(z_{i-1}-2z_i+z_{i+1})+\pi+z_{k-1}-z_k-z_{k+1}+z_{k+1}.$$

This is a telescoping sum; all terms cancel except 2π, as desired.

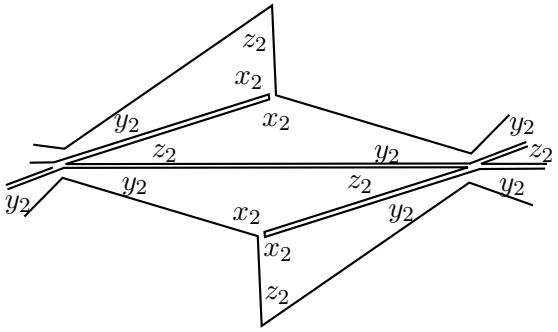

FIGURE 10.18. Labels from a hairpin turn

The angle sum around another such edge will be

$$z_{j-1} + 2y_j + \sum_{i=j+1}^{k-1} 2y_i + 2y_k + z_{k+1},$$

where j and k are hinge indices, with j between RL and k between LR, and $j < k$, and all 4-punctured spheres are labeled L between them. Again check that everything cancels except 2π.

We still need to consider the hairpin turns. With the gluing that comes from a hairpin turn, labels are as shown in figure 10.18, for the LL case. The cases RR, LR, RL are similar (exercise).

If we set $z_1 = 0$, the interior angle in which the 4-punctured sphere S_2 is bent at the hairpin turn, then all the equations in table 10.1 hold, depending on whether the hairpin turn occurs in the case LL, RR, LR, or RL. It remains only to check the edge equations. For the edge at the sharp bend, the equation will be identical to one of the previous equations, only now with angle $z_1 = 0$ included. The sum is still 2π. As for the final edges, in the case S_2 is R, these contribute $2z_2 + 4x_2 + \dots$, where the remainder of terms depends on whether the hairpin turn occurs at a hinge or not. In either case, the sum is 2π. Similarly when S_2 is L, and similarly for the outside hairpin turn that occurs at the 4-punctured sphere S_{C-1}.

We are now ready to show the space of angle structures is nonempty.

PROOF OF PROPOSITION 10.18. We show the space of angle structures is nonempty by showing there is a choice of $(z_1, z_2, \dots, z_{C-2}, z_{C-1})$ with $z_1 = z_{C-1} = 0$, all other $z_i \in (0, \pi)$, and $x_i, y_i \in (0, \pi)$. For this to hold, the equations in table 10.1 tell us that:

$$\begin{cases} 2z_i < z_{i-1} + z_{i+1} & \text{if } i \text{ is not a hinge } (LL \text{ or } RR) \\ |z_{i+1} - z_{i-1}| < \pi - z_i & \text{if } i \text{ is a hinge index } (LR \text{ or } RL) \end{cases} \tag{10.1}$$

The first equation is called the *convexity equation*. The second is the *hinge equation*.

We find a point with all $z_i \in (0, \pi)$ that satisfies convexity and hinge equations. Namely, let $z_1 = z_{C-1} = 0$. For each hinge index i, let $z_i = \pi/3$. Between hinge indices, choose a sequence to satisfy the convexity equations. For example, if j, k are consecutive hinge indices with $j < k$, then for all $j \leq i \leq k$, take

$$z_i = \frac{\pi}{3} - \frac{2(i-j)(k-i)}{(k-j)^2}.$$

Then the sequence $(z_1, z_2, \ldots, z_{C-2}, z_{C-1})$ satisfies all required conditions. Letting x_i and y_j be as in the tables, this gives an angle structure. □

COROLLARY 10.20. *Let $K[a_{n-1}, \ldots, a_1]$ be a 2-bridge knot or link with $a_i > 0$ for all i, or $a_i < 0$ for all i, and $|a_1| \geq 2$ and $|a_{n-1}| \geq 2$. Assume also that $n \geq 3$, so there are at least two twist regions in the diagram of K given by the denominator closure of the rational tangle $T(0, a_{n-1}, \ldots, a_1)$. Then $S^3 - K$ is hyperbolic.*

PROOF. The link complement $S^3 - K$ admits a triangulation as in proposition 10.13. Then proposition 10.18 implies the set of angle structures on this triangulation is nonempty. By theorem 8.28 in chapter 8, any manifold admitting an angle structure must also admit a hyperbolic structure. □

Corollary 10.20 is a special case of a stronger theorem due to Menasco determining when any alternating knot or link is hyperbolic [**Menasco, 1984**]. We will return to that theorem in chapter 11.

REMARK 10.21. Note that corollary 10.20 will also follow from theorem 10.17, which we will finish proving in the next section, by an appeal to theorem 9.13 (volume and angle structures). While the proof of corollary 10.20 given above appears short, in fact recall that the proof of theorem 8.28 requires the difficult hyperbolization theorem of Thurston, theorem 8.17, whose proof is beyond the scope of this book. By contrast, finishing the proof of theorem 10.17 requires only calculus and some calculations, and we go through it in the next section. Moreover, when finished, we will additionally know that the hyperbolic structure on 2-bridge links arises from a geometric triangulation of the link complements, and that triangulation can be explicitly described. Thus a proof of corollary 10.20 using the calculations in the next section is in many ways a "better" proof, worth finishing.

10.4. Maximum in interior

In this section we conclude the proof of theorem 10.17, by proving the following.

PROPOSITION 10.22. *For the 2-bridge links of proposition 10.18, the volume functional $\mathcal{V}\colon \mathcal{A}(\mathcal{T}) \to \mathbb{R}$ cannot have a maximum on the boundary of the space of angle structures.*

REMARK 10.23 (Summary of proof). The proof is given by a series of lemmas and calculations, and is quite technical. However, the idea of the proof is straightforward. First, we show that we can use the conditions on angle structures obtained in table 10.1; this is done in lemma 10.24. We then assume the maximum occurs on the boundary. Using the conditions of table 10.1, we find restrictions on the tetrahedra that arise; this is done in lemma 10.25. Finally, we show that in all cases that remain there is a path from the purported maximum on the boundary of the space of angle structures to the interior for which the directional derivative of $\mathcal{V}$ is strictly increasing. This contradicts the fact that the boundary point is a maximum.

Let K be a 2-bridge knot or link as in proposition 10.18. To obtain angle structures on $S^3 - K$, we made some simplifying assumptions in the proof of proposition 10.18. Namely, when constructing the triangulation $\mathcal{T}$, we had two tetrahedra T_i^1 and T_i^2 at each level, and we assumed that the angles on the two tetrahedra agreed. This led to the calculations of the previous section.

LEMMA 10.24. *The maximum of the volume functional $\mathcal{V}\colon \mathcal{A}(\mathcal{T}) \to \mathbb{R}$ must occur at a point for which the angles (x_i^1, y_i^1, z_i^1) of T_i^1 agree with those (x_i^2, y_i^2, z_i^2) of T_i^2, for all i, where T_i^1 and T_i^2 are the two tetrahedra constructed at the i-th level.*

PROOF. Suppose the volume is maximized at an angle structure A for which angles of T_i^1 and T_i^2 do not agree. Because of the symmetry of the construction of $\mathcal{T}$, note that we obtain a new angle structure A' by swapping angles of T_i^1 with the corresponding angles of T_i^2, for all tetrahedra of A. Note that since A and A' contain isometric ideal tetrahedra, $\mathcal{V}(A) = \mathcal{V}(A')$. Then A and A' are distinct angle structures, and the volume is maximized on both.

By theorem 9.9, the volume functional is strictly concave down on $\mathcal{A}(\mathcal{T})$. Thus if the volume obtains its maximum in the interior, then that maximum is unique, and the fact that $\mathcal{V}(A) = \mathcal{V}(A')$ gives an immediate contradiction in this case. If A lies on the boundary, then A' also lies on the boundary. Because $\mathcal{A}(\mathcal{T})$ is convex (proposition 9.11), the line between A and A' lies in $\mathcal{A}(\mathcal{T})$. But then along this line, the second directional derivative in the direction of the line is strictly negative, which implies the maximum cannot occur at the endpoints. This is a contradiction. □

By lemma 10.24, we may assume angles of T_i^1 and T_i^2 agree. Thus we may use the conditions on angles in table 10.1 that we calculated in the previous section to prove proposition 10.22.

Now assume that the maximum of $\mathcal{V}$ does occur on the boundary of the space of angle structures $\mathcal{A}(\mathcal{T})$. Then there will be a flat tetrahedron (or more accurately, a pair of flat tetrahedra). We will slowly narrow in on what type of tetrahedron it is, and where it occurs in the triangulation.

Note we will switch notation slightly. Rather than refering to the two tetrahedra between S_i and S_{i+1} as T_i^1 and T_i^2, we will simply refer to such a tetrahedron by Δ_i. Because the angles of T_i^1 and T_i^2 can be assumed to agree by lemma 10.24, this will simplify our notation.

LEMMA 10.25. *Suppose the maximum of the volume functional occurs on the boundary of $\mathcal{A}(\mathcal{T})$.*

1. *Then there exists a flat tetrahedron in the triangulation of the 2-bridge link.*
2. *The flat tetrahedron is not adjacent to any other flat tetrahedra.*
3. *The flat tetrahedron is not adjacent to a hairpin turn.*
4. *The flat tetrahedron occurs at a hinge, and satisfies $z_i = \pi$, and for the two adjacent tetrahedra, $z_{i-1} = z_{i+1}$.*
5. *If some tetrahedron Δ_i is type LL or RR, then Δ_{i-1} and Δ_{i+1} cannot both be flat.*

PROOF. By proposition 9.19, if the volume takes its maximum at an angle structure for which a tetrahedron has an angle equal to 0, then it must have two angles equal to 0 and one equal to π. This is a flat tetrahedron. Because we are assuming the maximum is on the boundary, there must be a flat tetrahedron in the triangulation, say tetrahedron Δ_i is flat, where $2 \leq i \leq C-2$. This proves item (1).

There are three cases for the angles: (x_i, y_i, z_i) can equal $(0, 0, \pi)$, $(0, \pi, 0)$, or $(\pi, 0, 0)$. There are also four possibilities for the tetrahedron: type LL, RR, LR, or RL. The equations of table 10.1 give us angles of adjacent tetrahedra in all cases, and an analysis of these will lead to the conclusions of the lemma.

Case $(x_i, y_i, z_i) = (0, 0, \pi)$.

LL, RR: Equations of table 10.1 imply

$$0 = \frac{1}{2}(2\pi - z_{i-1} - z_{i+1}), \text{ which implies } z_{i-1} = z_{i+1} = \pi.$$

In this case, both adjacent tetrahedra must be flat.

LR, RL: Equations of table 10.1 imply

$$0 = \frac{1}{2}(z_{i+1} - z_{i-1}), \text{ or } z_{i-1} = z_{i+1}.$$

Note in this case, it is not necessarily true that both adjacent tetrahedra are flat, but if one is flat then so is the other.

Case $(x_i, y_i, z_i) = (0, \pi, 0)$. .

LL: $0 = \frac{1}{2}(2\pi - z_{i-1} - z_{i+1})$ implies $z_{i-1} = z_{i+1} = \pi$.

RR: $0 = \frac{1}{2}(z_{i-1} + z_{i+1})$ implies $z_{i-1} = z_{i+1} = 0$.

LR: $0 = \frac{1}{2}(\pi - z_{i-1} + z_{i+1})$ implies $\pi + z_{i+1} = z_{i-1}$. Since angles lie in $[0, \pi]$, it follows that $z_{i+1} = 0$ and $z_{i-1} = \pi$.

RL: Similar to the last case, $z_{i+1} = \pi$ and $z_{i-1} = 0$.
For all types of tetrahedra in this case, the the two tetrahedra adjacent to Δ_i are flat.

Case $(x_i, y_i, z_i) = (\pi, 0, 0)$.

LL: Equations of table 10.1 imply $z_{i-1} = z_{i+1} = 0$.
RR: $z_{i-1} = z_{i+1} = \pi$.
LR: $z_{i-1} = 0$, $z_{i+1} = \pi$.
RL: $z_{i+1} = 0$, $z_{i-1} = \pi$.
Again this shows that the two adjacent tetrahedra are both flat in this case.

In all cases, if two adjacent tetrahedra are flat, then the next adjacent tetrahedron is also flat. It follows that if there are two adjacent flat tetrahedra, then all tetrahedra are flat, and the structure has zero volume, which cannot be a maximum for the volume. Thus we cannot have two adjacent flat tetrahedra. This proves item (2).

Moreover, the only case that does not immediately imply multiple adjacent flat tetrahedron is the first case, with $z_i = \pi$, for the hinge tetrahedra *RL* or *LR*, and the calculation above gives the relationship $z_{i-1} = z_{i+1}$, proving item (4).

If the tetrahedron is adjacent to a hairpin turn, then $i = 2$ or $i = C - 2$, and $z_i = \pi$. We also have $z_1 = 0$ and $z_{C-1} = 0$, hence in either case the equations above imply that a next adjacent tetrahedron, corresponding to z_3 or z_{C-3}, is flat, and thus all tetrahedra are flat, contradicting item (2). This proves (3).

Now suppose Δ_{i-1} and Δ_{i+1} are flat. By the previous work, we know $z_{i-1} = z_{i+1} = \pi$. If Δ_i is type *LL*, the equations of table 10.1 imply $x_i = \frac{1}{2}(2\pi - \pi - \pi) = 0$, so Δ_i is flat. Similarly if Δ_i is of type *RR*, then $y_i = 0$ and Δ_i is flat. But then we have three adjacent flat tetrahedra, contradicting item (2). This proves item (5). □

We now know that any flat tetrahedron occurring in a maximum for $\mathcal{V}$ on the boundary has a very particular form. To finish the proof of proposition 10.22, we will show that the maximum cannot occur in the remaining cases. For the argument, we will find a path through the space of angle structures starting at the purported maximum for $\mathcal{V}$ on the boundary, and then show that the derivative at time 0 in the direction of this path is strictly positive. This will contradict the fact that the point is a maximum.

The paths we consider adjust the angles of the flat tetrahedron Δ_i by

$$(x_i(\epsilon), y_i(\epsilon), z_i(\epsilon)) = ((1 + \lambda)\epsilon, (1 - \lambda)\epsilon, \pi - 2\epsilon),$$

where $\epsilon \to 0$ and λ will be a carefully chosen constant. In such a path, we will leave as many angles unchanged away from the i-th tetrahedron as possible. However, the equations in table 10.1 imply that many angles of adjacent tetrahedra must change with ϵ as well.

Recall from lemma 9.15 that the derivative of the volume functional in the direction of a vector $w = (w_1, \ldots, w_n)$ at a point $a = (a_1, \ldots, a_n)$ is

$$\frac{\partial \mathcal{V}}{\partial w} = \sum_{i=1}^{3n} -w_i \log \sin a_i.$$

The terms of the sum are grouped into threes, with each group corresponding to a single tetrahedron, with derivative coming from theorem 9.9.

LEMMA 10.26. *Let $\gamma(t)$ be a path through $\overline{\mathcal{A}(\mathcal{T})}$ with the angles of the i-th tetrahedron Δ_i in $\gamma(t)$ satisfying $(x_i, y_i, z_i) = ((1+\lambda)t, (1-\lambda)t, \pi - 2t)$. Then the derivative of the volume of Δ_i along this path at $t = 0$ satisfies*

$$\left.\frac{d \operatorname{vol}(\Delta_i)}{dt}\right|_{t=0} = \log\left(\frac{4}{1-\lambda^2}\left(\frac{1-\lambda}{1+\lambda}\right)^{\lambda}\right).$$

PROOF. By theorem 9.9, the derivative in the direction of $\gamma'(0) = w = ((1+\lambda), (1-\lambda), -2)$ is

$$\begin{aligned}\frac{\partial \operatorname{vol}}{\partial w} = \lim_{t\to 0} \big[&- (1+\lambda)\log\sin((1+\lambda)t) - (1-\lambda)\log\sin((1-\lambda)t) \\ &+ 2\log\sin(\pi - 2t)\big].\end{aligned}$$

Using the Taylor expansion $\sin(At) = At$ near $t = 0$, this becomes

$$\begin{aligned}\frac{\partial \operatorname{vol}}{\partial w} &\lim_{t\to 0} \big[- (1+\lambda)\log((1+\lambda)t) - (1-\lambda)\log((1-\lambda)t) + 2\log(2t)\big] \\ &= \log\left(\frac{4}{(1+\lambda)(1-\lambda)}\left(\frac{1-\lambda}{1+\lambda}\right)^{\lambda}\right)\end{aligned}$$

□

We denote the location of a flat tetrahedron by a vertical line:

$$\ldots LL|RR \ldots.$$

By lemma 10.25, a vertical line can only appear at a hinge: $L|R$ or $R|L$; at least two letters lie between consecutive vertical lines; and patterns $L|RR|L$ and $R|LL|R$ cannot occur. The remaining cases are $LR|LR$ and $RL|RL$, which we deal with simultaneously; $RR|LR$ and $LL|RL$ and their reversals $RL|RR$ and $LR|LL$; and $RR|LL$ and $LL|RR$.

In all cases, we find a path $\gamma(t)$ through $\mathcal{A}(\mathcal{T})$ with $\gamma(0)$ a point on the boundary with the flat tetrahedron specified in the given case.

Case $LR|LR$ and $RL|RL$: Begin with the $LR|LR$ case. Let Δ_i denote the flat tetrahedron, with $(x_i, y_i, z_i) = (0, 0, \pi)$. We take a path $\gamma(t)$ to satisfy $(x_i(t), y_i(t), z_i(t)) = (t, t, \pi - 2t)$, i.e. $\lambda = 0$ in lemma 10.26, and we will keep as many other angles constant as possible. The formulas in table 10.1 imply that angles of tetrahedra Δ_{i-1} and Δ_{i+1} must also vary, as in the following table. In the table, we let $z_{i-1} = z_{i+1} = w$ (required by lemma 10.25(4)), and we let $u = z_{i-2}$, $v = z_{i+2}$.

Angle	Δ_{i-1}	Δ_i	Δ_{i+1}
x	$\frac{1}{2}(2\pi - u - w - 2t)$	t	$\frac{1}{2}(2t - w + v)$
y	$\frac{1}{2}(u - w + 2t)$	t	$\frac{1}{2}(2\pi - 2t - w - v)$
z	w	$\pi - 2t$	w

Thus the derivative vector to the path at time $t = 0$ is

$$\gamma'(t) = (0, \dots, 0, \underbrace{-1, 1, 0}_{\Delta_{i-1}}, \underbrace{1, 1, -2}_{\Delta_i}, \underbrace{1, -1, 0}_{\Delta_{i+1}}, 0, \dots, 0).$$

Hence the derivative of the volume functional in the direction of the path is given by

$$\begin{aligned}\left.\frac{d\mathcal{V}}{dt}\right|_{t=0} &= \log\sin\left(\frac{1}{2}(2\pi - u - w)\right) - \log\sin\left(\frac{1}{2}(u - w)\right) + \log 4 \\ &\quad - \log\sin\left(\frac{1}{2}(v - w)\right) + \log\sin\left(\frac{1}{2}(2\pi - v - w)\right) \\ &= \log\left(\frac{4\sin(u/2 - w/2)\sin(v/2 - w/2)}{\sin(u/2 + w/2)\sin(v/2 + w/2)}\right) > 0.\end{aligned}$$

Note this is strictly positive, hence the volume functional cannot have a maximum at this boundary point. The calculation is similar for $RL|RL$.

Remaining cases: We will first take care of cases $RR|LR$ and $RR|LL$.

As in the previous case, we will take a path such that the flat tetrahedron Δ_i changes. This time, we will find a fixed λ such that angles of Δ_i satisfy $(x_i, y_i, z_i) = ((1 - \lambda)t, (1 + \lambda)t, \pi - 2t)$ for $t \in [0, \epsilon]$, for some $\epsilon > 0$. At time $t = 0$, we require $z_{i-1} = z_{i+1} = w$, a constant. Set $z_{i-2} = u$ and $z_{i+2} = v$, also constant. Additionally, adjust z_{i-1} so that at time t, $z_{i-1} = w - 2\lambda t$. In the argument below, we will assume that $i - 2 \neq 1$, so there is a tetrahedron Δ_{i-2}. We also need to consider the case $i - 2 = 1$; we will do this at the very end of the proof. Assuming $i - 2 \neq 1$, the angles that are modified are shown in the tables below for the cases $RR|LR$ and $RR|LL$.

		R	R	$\mid$	L	R
Angle	Δ_{i-2}		Δ_{i-1}	Δ_i		Δ_{i+1}
x	$A + \frac{1}{2}w - \lambda t$		$x_{i-1}(t, \lambda)$	$(1 + \lambda)t$		$x_{i+1}(t, \lambda)$
y	$A' - \frac{1}{2}w + \lambda t$		$\frac{1}{2}(\pi - 2t)$	$(1 - \lambda)t$		$\frac{1}{2}(2t - w + v)$
z	u		$w - 2\lambda t$	$\pi - 2t$		w

		R	R	$\mid$	L	L
Angle	Δ_{i-2}		Δ_{i-1}	Δ_i		Δ_{i+1}
x	$A + \frac{1}{2}w - \lambda t$		$x_{i-1}(t, \lambda)$	$(1 + \lambda)t$		$\frac{1}{2}(\pi + 2t - v)$
y	$A' - \frac{1}{2}w + \lambda t$		$\frac{1}{2}(\pi - 2t)$	$(1 - \lambda)t$		$y'_{i+1}(t, \lambda)$
z	u		$w - 2\lambda t$	$\pi - 2t$		w

Here A and A' are constants, $x_{i-1}(t,\lambda) = \frac{1}{2}(u - 2w + 4\lambda t + \pi - 2t)$, $x_{i+1}(t,\lambda) = \frac{1}{2}(2\pi - 2t - w - v)$, and $y'_{i+1}(t,\lambda) = \frac{1}{2}(\pi - 2t - 2w + v)$.

If $i > 3$, we may use the table to compute the derivative in the direction of the path, and find in the case $RR|LR$, $d\mathcal{V}/dt|_{t=0}$ equals:

(10.2)
$$\left.\frac{d\mathcal{V}}{dt}\right|_{t=0} = \log\left(\frac{4}{1-\lambda^2}\frac{\sin(\frac{v}{2}+\frac{w}{2})}{\sin(\frac{v}{2}-\frac{w}{2})}\frac{\sin x_{i-1}}{\sin y_{i-1}}\left(\frac{1-\lambda}{1+\lambda}\cdot\frac{\sin x_{i-2}}{\sin y_{i-2}}\frac{\sin^2 z_{i-1}}{\sin^2 x_{i-1}}\right)^{\lambda}\right).$$

And in the case $RR|LL$, $d\mathcal{V}/dt|_{t=0}$ equals:

(10.3)
$$\left.\frac{d\mathcal{V}}{dt}\right|_{t=0} = \log\left(\frac{4}{1-\lambda^2}\frac{\sin x_{i-1}}{\sin y_{i-1}}\frac{\sin y_{i+1}}{\sin x_{i+1}}\left(\frac{1-\lambda}{1+\lambda}\cdot\frac{\sin x_{i-2}}{\sin y_{i-2}}\frac{\sin^2 z_{i-1}}{\sin^2 x_{i-1}}\right)^{\lambda}\right).$$

LEMMA 10.27. *Let X, Y be positive constants, and let*

$$f(\lambda) = \log\left(\frac{4}{1-\lambda^2}\,X\left(\frac{1-\lambda}{1+\lambda}\,Y\right)^{\lambda}\right).$$

Then f has a critical point at $\lambda = (Y-1)/(Y+1)$, and f takes the value $\log(X(Y+1)^2/Y)$ at this point.

PROOF. Calculus. □

Now apply lemma 10.27 to equation (10.2) and equation (10.3), choosing λ to be the value given by that lemma at time $t = 0$. For this value of λ, we obtain the following:

The derivative $d\mathcal{V}/dt|_{t=0}$ in the case $RR|LR$ equals:

(10.4)
$$\log\left(\frac{\sin(\frac{v}{2}+\frac{w}{2})}{\sin(\frac{v}{2}-\frac{w}{2})}\frac{\sin x_{i-1}}{\sin y_{i-1}}\left(1+\frac{\sin x_{i-2}}{\sin y_{i-2}}\frac{\sin^2 z_{i-1}}{\sin^2 x_{i-1}}\right)^2\frac{\sin y_{i-2}}{\sin x_{i-2}}\frac{\sin^2 x_{i-1}}{\sin^2 z_{i-1}}\right)$$
$$\geq \log\left(\frac{\sin x_{i-1}}{\sin y_{i-1}}\left(1+\frac{\sin x_{i-2}}{\sin y_{i-2}}\frac{\sin^2 z_{i-1}}{\sin^2 x_{i-1}}\right)^2\frac{\sin y_{i-2}}{\sin x_{i-2}}\frac{\sin^2 x_{i-1}}{\sin^2 z_{i-1}}\right).$$

The derivative $d\mathcal{V}/dt|_{t=0}$ in the case $RR|LL$ equals:

(10.5)
$$\log\left(\frac{\sin x_{i-1}}{\sin y_{i-1}}\frac{\sin y_{i+1}}{\sin x_{i+1}}\left(1+\frac{\sin x_{i-2}}{\sin y_{i-2}}\frac{\sin^2 z_{i-1}}{\sin^2 x_{i-1}}\right)^2\frac{\sin y_{i-2}}{\sin x_{i-2}}\frac{\sin^2 x_{i-1}}{\sin^2 z_{i-1}}\right).$$

The remaining quantities $\sin a/\sin b$ are geometric: by the law of sines, they give a ratio of lengths of triangles, and the triangles are those from our cusp triangulation, as in figure 10.14.

LEMMA 10.28. *In the case $RR|L$, let P, Q, T be the lengths of segments on the middle zigzag R, with P opposite the angle x_{i-1}, Q opposite the angle*

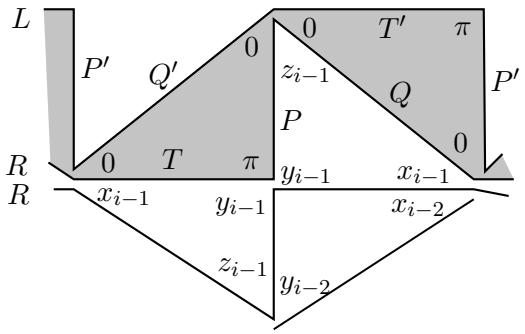

FIGURE 10.19. Segments of length P, Q, and T shown on the zigzag corresponding to the first R after a flat hinge tetrahedron. For the $RR|LL$ case, segments of length P', Q' and T' also shown on the first L zigzag after the flat hinge tetrahedron.

y_{i-1} and T opposite the angle z_{i-1}, as in figure 10.19. Then the following hold:

$$\frac{\sin x_{i-2}}{\sin y_{i-2}} \frac{\sin^2 z_{i-1}}{\sin^2 x_{i-1}} = \frac{T}{P}, \qquad \frac{\sin x_{i-1}}{\sin y_{i-1}} = \frac{P}{Q}.$$

PROOF. The equations follow from the law of sines. □

LEMMA 10.29. *Suppose there is a subword $L|R^kL$ with $k \geq 2$. Let Q, P, and T be lengths of segments of the zigzag corresponding to the first R, with P and T adjacent to the angle labeled $z = \pi$ on the hinge tetrahedron $L|R$. Then $P + T > Q$.*

Similarly, if there is a subword $R|L^kR$ with $k \geq 2$, and Q', P', and T' denote the lengths of the segments of the zigzag corresponding to the first L, with P' and T' adjacent to the angle $z = \pi$ on the hinge tetrahedron $R|L$, then $P' + T' > Q'$.

The labels P, Q, and T are illustrated in figure 10.19. In the case there are at least two L's at the top of the figure, P', Q' and T' will be labeled as shown there as well.

PROOF. [**Guéritaud, 2006**, Lemma 8.2]. □

Now we can show in the $RR|LR$ case the derivative $d\mathcal{V}/dt|_{t=0}$ is positive. From equation (10.4), we obtain

$$\left.\frac{d\mathcal{V}}{dt}\right|_{t=0} \geq \log\left(\frac{P}{Q}\left(1 + \frac{T}{P}\right)^2 \frac{P}{T}\right) = \log\left(\frac{P+T}{T} \cdot \frac{P+T}{Q}\right) > \log(1) = 0.$$

A similar calculation holds in the $LL|RL$ case. By swapping the indices $i-1$, $i+1$, and $i-2$, $i+2$, the same argument shows the derivative is strictly positive in the $RL|RR$ and $LR|LL$ cases, provided $i+2$ is not the index of a hairpin turn.

We now finish the $RR|LL$ case.

LEMMA 10.30. *In the $RR|LL$ case, with P', Q', and T' as in figure 10.19, $P'/T' = T/P$, and $\sin(y_{i+1})/\sin(x_{i+1}) = P'/Q'$.*

PROOF. By lemma 10.25, item (5), there is no flat tetrahedron either directly before or directly after the sequence $RR|LL$, so the angles of Δ_{i-2}, Δ_{i-1}, Δ_{i+1}, and Δ_{i+2} are all positive. Thus the parameter w can vary freely in an open interval when $t = 0$. Since the volume is maximized, the derivative with respect to w satisfies

$$\left.\frac{d\mathcal{V}}{dw}\right|_{t=0} = \log\left(\sqrt{\frac{\sin x_{i-2}}{\sin y_{i-2}}} \cdot \frac{\sin z_{i-1}}{\sin x_{i-1}} \cdot \frac{\sin z_{i+1}}{\sin y_{i+1}} \cdot \sqrt{\frac{\sin y_{i+2}}{\sin x_{i+2}}}\right) = 0.$$

Thus

$$\frac{\sin y_{i-2} \sin^2 x_{i-1}}{\sin x_{i-2} \sin^2 z_{i-1}} \cdot \frac{\sin^2 y_{i+1} \sin x_{i+2}}{\sin^2 z_{i+1} \sin y_{i+2}} = 1.$$

Using an expanded version of figure 10.19, one can check (exercise) that

$$\frac{\sin y_{i-2} \sin^2 x_{i-1}}{\sin x_{i-2} \sin^2 z_{i-1}} = \frac{P}{T}, \quad \text{and} \quad \frac{\sin^2 y_{i+1} \sin x_{i+2}}{\sin^2 z_{i+1} \sin y_{i+2}} = \frac{P'}{T'}.$$

This shows $P'/T' = T/P$.

Similarly using figure 10.19, one can check that $\sin(y_{i+1})/\sin(x_{i+1}) = P'/Q'$. □

By lemma 10.30 and equation (10.5), we find that in the $RR|LL$ case,

$$\begin{aligned}
\left.\frac{d\mathcal{V}}{dt}\right|_{t=0} &= \log\left(\frac{P}{Q}\frac{P'}{Q'}\left(1+\frac{T}{P}\right)^2\frac{P}{T}\right) \\
&= \log\left(\frac{P}{Q}\left(1+\frac{T}{P}\right)\frac{P'}{Q'}\left(1+\frac{P'}{T'}\right)\frac{T'}{P'}\right) \\
&= \log\left(\frac{P+T}{Q}\cdot\frac{P'+T'}{Q'}\right) \\
&> \log(1) = 0.
\end{aligned}$$

A similar calculation takes care of the $LL|RR$ case.

So far, we have argued only for $i > 3$. It remains to consider what happens when $i = 3$. In this case, $i - 2 = 1$ is the index of a hairpin turn, and the terms $\sin y_1/\sin x_1$ disappear from the computations of $d\mathcal{V}/dt$ in equation (10.2) and equation (10.3). We have a result similar to lemma 10.29: R^aL is a tessellated Euclidean triangle, and lengths still behave as in lemma 10.29 to give the same result; see [**Guéritaud, 2006**, Lemma 1.5].

This concludes the proof of proposition 10.22. □

We now assemble the pieces to obtain the stronger result of theorem 10.17.

PROOF OF THEOREM 10.17. Let K be a knot or link complement with a reduced alternating diagram with at least two twist regions. Let $\mathcal{T}$ be the triangulation of $S^3 - K$ described in this chapter. By proposition 10.18, the space of angle structures $\mathcal{A}(\mathcal{T})$ is nonempty. By proposition 10.22, the volume functional $\mathcal{V}\colon\ \mathcal{A}(\mathcal{T}) \to \mathbb{R}$ cannot have a maximum on the boundary of the space of angle structures. It follows that the maximum of $\mathcal{V}$ is on the interior of the space of angle structures. Let $A \in \mathcal{A}(\mathcal{T})$ denote this critical point. Thus by theorem 9.13 (volume and angle structures), the ideal hyperbolic tetrahedra obtained from the angle structure A give $S^3 - K$ a complete hyperbolic structure. Note since A lies in the interior, the ideal hyperbolic tetrahedra it determines are all positively oriented, as claimed. □

10.5. Exercises

EXERCISE 10.1. Sketch rational tangles and diagrams of 2-bridge links associated to the following continued fractions: $[3, 2]$, $[0, 3, 2]$, $[1, 3, 2]$.

EXERCISE 10.2. Continued fractions. Show every rational number has a continued fraction expansion $p/q = [a_n, a_{n-1}, \ldots, a_1]$ such that if $i < n$, then $a_i \neq 0$, and such that if $p/q > 0$, then each $a_i \geq 0$, while if $p/q < 0$, then each $a_i \leq 0$.

EXERCISE 10.3. Prove lemma 10.9. That is, show that if $K[a_{n-1}, \ldots, a_1]$ is a 2-bridge knot or link, then we may assume that $|a_{n-1}| \geq 2$ and $|a_1| \geq 2$.

EXERCISE 10.4. Work through the identification of tetrahedra at the innermost crossing. Prove that faces of the innermost tetrahedra are glued in pairs, two triangles of one tetrahedron glued to triangles of the opposite tetrahedron. Why is there no need to consider both horizontal and vertical crossings for the innermost crossing?

EXERCISE 10.5. In proposition 10.13, we require at least two twist regions. Show that this requirement is necessary by showing that the construction fails to give a triangulation of a knot or link with just one twist region. What breaks down?

EXERCISE 10.6. This exercise asks you to consider hairpin turns.

(1) Prove if $|a_{n-1}| \geq 3$, there is a 3-valent vertex of the cusp triangulation.
(2) Prove all vertices aside from possibly a single vertex in a hairpin turn must have valence at least four.
(3) If $|a_{n-1}| = 2$, prove the vertex corresponding to the outside hairpin turn may have arbitrarily high valence.

EXERCISE 10.7. Use the methods of this chapter to find the form of the cusp triangulation for the twist knot $J(2, n)$. How many tetrahedra are in its decomposition?

EXERCISE 10.8. Find the form of the cusp triangulation for $J(k, \ell)$, where one of k, ℓ is even. How many tetrahedra are in its decomposition?

EXERCISE 10.9. Find the form of the cusp triangulation of a 2-bridge knot with exactly three twist regions.

EXERCISE 10.10. Prove lemma 10.19: that pleating angles as in figure 10.16 satisfy $\alpha_1 + \alpha_2 - \alpha_3 = 0$ when the cusp is Euclidean.

EXERCISE 10.11. Determine the labels of the hairpin turns of the form RR, LR, RL, similar to figure 10.18.

EXERCISE 10.12. In the cases $RR|LR$ and $RR|LL$, compute the derivative $d\mathcal{V}/dt|_{t=0}$ and check that it agrees with the formulas given in equation (10.2) or equation (10.3).

EXERCISE 10.13. Give the proof of lemma 10.29.

EXERCISE 10.14. Work through the geometric details of lemma 10.30: Sketch the zigzag labeled L at the top of figure 10.19, along with angles at its corners, and show that:

$$\frac{\sin y_{i-2} \sin^2 x_{i-1}}{\sin x_{i-2} \sin^2 z_{i-1}} = \frac{P}{T}, \quad \text{and} \quad \frac{\sin^2 y_{i+1} \sin x_{i+2}}{\sin^2 z_{i+1} \sin y_{i+2}} = \frac{P'}{T'}.$$

Also show $\sin(y_{i+1})/\sin(x_{i+1}) = P'/Q'$.

EXERCISE 10.15. Go carefully through the proof of cases $RR|LR$ and $RR|LL$ when the index of the flat tetrahedron is $i = 3$.